Hindawi
Shock and Vibration
Volume 2021, Article ID 8860493, 11 pages
https://doi.org/10.1155/2021/8860493

Research Article

Influence of Balance Hole Diameter on Leakage Flow of the Balance Chamber in a Centrifugal Pump

Wei Dong,[1,2] Diyi Chen ,[1,2] Jian Sun,[1,2] Yan Dong,[1,2] Zhenbiao Yang,[3] and Junle Yan[3]

[1]*Key Laboratory of Agricultural Soil and Water Engineering in Arid and Semiarid Areas, Ministry of Education, Northwest A&F University, Yangling, Xianyang 712100, China*
[2]*Institute of Water Resources and Hydropower Research, Northwest A&F University, Yangling, Xianyang 712100, China*
[3]*Hanjiang-to-Weihe River Water Diversion Project Construction Co., Ltd., Xi'an 710010, Shaanxi, China*

Correspondence should be addressed to Diyi Chen; diyichen@nwsuaf.edu.cn

Received 10 September 2020; Revised 30 November 2020; Accepted 17 December 2020; Published 8 February 2021

Academic Editor: Yong Zhu

The balancing holes in centrifugal pumps with seals mounted in both suction and discharge sides are one of the approaches used by pump manufacturers to reduce the axial thrust. The balance hole diameter directly affects the axial force of the centrifugal pump. The flow characteristics in the balance chamber are closely related to the balance hole diameter. However, research is not very clear on the internal flow of the balanced chamber, due to the small axial and radial sizes and the complicated flow conditions in the chamber. In this paper, we analyzed the influence of the balance hole diameter on the liquid leakage rate, flow velocity, and vortex motion in the balance chamber. The results indicated that when the balance hole diameter was lower than the design value, the volume flow rate of leakage flow was proportional to the diameter. The liquid flow rate and vortex distribution rules in the balance chamber were mainly associated with the coeffect of radial leakage flow in the rear sealing ring interval and the axial balance hole leakage flow. The research has revealed the mechanisms of leakage flow of the balance chamber in the centrifugal pump and that this is of great significance for accurate calculation and balancing of the axial force.

1. Introduction

Calculating and balancing the axial forces of a centrifugal pump are the main challenges in the pump industry in recent years. For the seals mounted in both suction and discharge sides of the impeller with balance holes in a centrifugal pump, the lateral chamber of the impeller back cover plate is composed to the rear chamber and the balance chamber. The balance chamber is connected to the impeller entrance through the balance hole which is widely employed to balance axial forces in a centrifugal pump [1, 2]. To calculate the axial force in the centrifugal pump, current theoretical formulas always assume that the liquid in the impeller cover plate lateral chamber has no leakage flow, and the liquid in the balance chamber has no rotational motion [3]. The numerical results of the axial force of the centrifugal pump, which is calculated from classical theory in given conditions, are inconsistent with the test results from the physical experiments [4]. On the other hand, pressures in the area above the sealing ring of the impeller in the pump, the front chamber, and the rear chamber offset one another [5]. Therefore, in the area below the sealing ring, the characteristics of the flow in the balance chamber are closely related to the axial force of the centrifugal pump. Meanwhile, the characteristics of the flow in the lateral cavity of the centrifugal pump impeller cover plate have a significant influence on centrifugal pump performance, volume loss, and disc friction loss [6, 7]. In light of this, a study on the volume flow rate of the leakage flow in the balance chamber and the corresponding flow characteristics would help enlarge the understanding of the axial force of the centrifugal pump and the corresponding production of flow loss. This is of significance for achieving accurate axial force calculations.

Due to the centrifugal force, the liquid in the balance chamber rotates with the impeller. When the balance hole is open, the flow in the balance chamber (which is the main

stream) is caused by the simultaneous flow of the impeller rotation and the leakage flow from the balance hole in the numerical study [8]. A numerical study found that the volume flow rate of the leakage flow directly affected the liquid pressure in the balance chamber, and the calculation of the impeller cover plate force (i.e., the axial force of the centrifugal pump) and an appropriate balance hole diameter could balance the axial force to its maximum [9]. Other studies [10–16] found that the characteristics of leakage flow in the balance chamber directly influence the accuracy of the axial force prediction. Other studies [17, 18] on the centrifugal pump have concluded that the distribution of axial velocity in the lateral chamber of the back cover plate is similar to that in the closed cylinder. This demonstrates the existence of turbulent boundary layers near the outer wall of the impeller back cover plate and the fixed inner wall. In addition, a core flow area can be found between two layers, with the core velocity varying slightly along the axial direction [19–24]. Therefore, the flow field distribution at the axial center of the balance chamber reflects the overall distribution of flow in the core flow area of the balance chamber.

Numerical calculation is an extensive and accurate method for studying the centrifugal pump. Interesting research has been undertaken in this area; for example, a numerical calculation method can be used to predict the performance of the centrifugal pump and the simulation results agree with the measured results [25–27]. The pressure distribution at the side of the impeller cover plate was obtained by numerical calculation, and the predicted axial force of the centrifugal pump was compared with the test results. It was concluded that numerical prediction of axial force was highly accurate [28–30].

Using the above discussions as motivation, the main concepts of this paper can be classified into three topics. Firstly, the correlation between the diameter of the balance hole, the liquid leakage, and the vortex of the balance chamber is revealed. Secondly, the main factors affecting the liquid flow velocity and vortex distribution in the balance chamber are obtained. Thirdly, the liquid flow velocity and the vortex distribution in a balance chamber with six balance hole diameters are analyzed in detail.

2. Pump Simulation

2.1. Model Pump. The design parameters of the centrifugal pump in this study are as follows: quantity of flow $Q = 200\ \mathrm{m}^3/\mathrm{h}$, head of delivery $H = 32$ m, efficiency $\eta = 81\%$, rotational speed $n = 1450$ r/min, external impeller diameter $D = 325$ mm, seal clearance $b = 0.22$ mm, back seal ring diameter $D_n = 165$ mm, impeller hub diameter $D_h = 60$ mm, balance hole diameter $d = 8$ mm, and the number of the balance hole $z = 6$.The centrifugal pump model is shown in Figure 1.

2.2. Calculation Method. The flow field was solved using the software FLUENT. Grid interfaces were established between the impellers, the volute, the seal clearance, the impeller cover plate, the lateral chamber, and the balance hole to allow for data transmission between different computational domains. The inlet boundary condition was defined to have constant velocity, and the outlet boundary was set as a free outflow condition. A nonslipping condition was adopted for the solid surface, and the standard wall function was applied to calculate the turbulent flows near the near wall. The distribution of velocity near the impeller cover plate wall in the balance chamber area is shown in Figure 2.

The flow in the pump was assumed to be incompressible and steady. At present, the numerical methods for solving three-dimensional Navier–Stokes equations can be divided into three categories: direct simulation (DNS); large eddy simulation (LES); and the simulation method of the mean when using Reynolds equation. The first two methods cannot be implemented on ordinary computers because of their high computational requirements. In comparison, although the accuracy of the Reynolds time-average method is lower, it has low requirements for computing equipment. Therefore, the Reynolds time-average method is widely used, and the numerical simulation of the internal flow field of the impeller is largely based on this method. The RNG turbulence model was adopted. The time-averaged continuity equation and the Navier–Stokes equations of the relative coordinate system were solved during the simulation, and the SIMPLEC algorithm was adopted to achieve the coupling of pressure and velocity. The difference schemes were set as follows: the pressure subrelaxation item is in the standard format, and the momentum subrelaxation item, turbulent energy subrelaxation item, turbulent energy dissipation subrelaxation item, and turbulent energy dissipation rate are all Second-Order Upwind Difference Scheme dispersion difference equations. The following are the coefficients in the iterative calculation of algebraic equations: the subrelaxation coefficient for pressure, which is 0.3; the momentum, which is 0.7; the turbulence energy, which is 0.8; and the turbulence energy dissipation rate, which is 0.8.

2.3. Grid Independence and Performance Verification. Mixed grids were adopted for the integral pump, and structural grids were adopted for the impeller back cover plate lateral chamber area. During the simulation, the study of grid independence is commonly a necessary step for the simulation to ensure the accuracy and reliability of the computational fluid dynamics (CFD) results, especially for the grids with structural elements [15–17]. This paper refined the grids in the back cover plate lateral chamber during the grid independence study to eliminate the influence of the grid number on the flow field in the balance chamber area of the centrifugal pump. The η (efficiency) of the pump is determined by all of its H (head), Q (flow rate), and P (shaft power). Therefore, the grid independence validation of the head and the efficiency are completed in this step. The variations of the head and the efficiency over different grid numbers of the centrifugal pump (grid numbers were increased from 1.46 million to 4.13 million) are shown in Figure 3. The computational grid model of the centrifugal pump is shown in Figure 4.

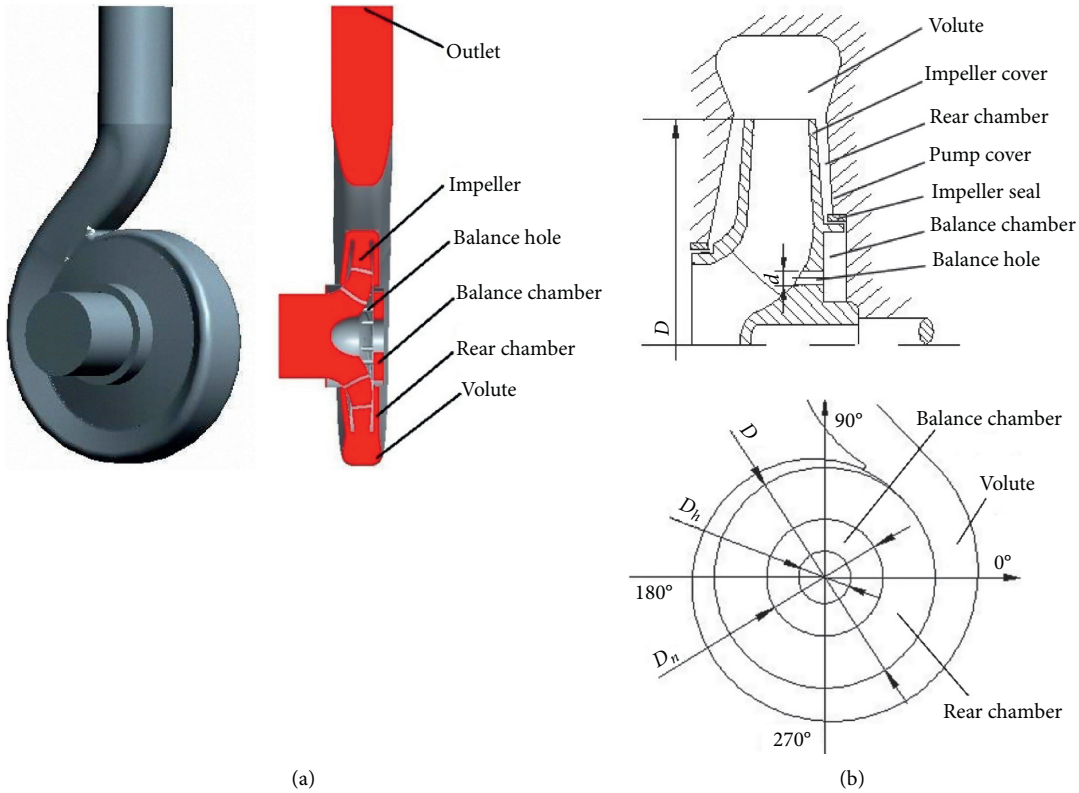

Figure 1: Geometric model. (a) Physical model. (b) Sketch of the centrifugal pump.

We see in Figure 3 that the increase of the overall grid number induces slight variation of the head and the efficiency of the pump. The head and the efficiency almost remain unchanged when the grid number reaches 3.22 million. In light of this, the grids of the centrifugal pump adopt 3.22 million elements, in which about 1.22 million grids are for the balance chamber area. The same topology is adopted for all the models with different balance hole diameters, and the overall grid numbers of different models are generally equivalent to one another. The numerical results were compared with the test results in the head and the efficiency of the centrifugal pump, seen in Figure 5.

Figure 5 shows that, in the work area 160–240 m^3/h, the relative errors of the numerical and test results on the head and efficiency are within 3% and 2%, respectively. The numerical results of the performance of the centrifugal pump are consistent with the test results. The numerical results of the centrifugal pump with different balance hole diameters are shown in Table 1.

From Table 1, under design conditions, the numerical simulation values of the head and efficiency of the pump ($d = 8$ mm) are both higher than its experimental values with relative errors of 2.72% and 1.53%, respectively. For the remaining five models, impeller balance hole diameter only changes within the range of 0 mm and 12 mm, leading to mild changes on the external characteristics of the pump. The design parameters of the centrifugal pump agree well with the test results. The numerical results are generally close to the test results, which demonstrates the reliability of the numerical calculation results.

3. Calculation Results and Analysis

3.1. Analysis of Leakage in the Balance Chamber. Figure 6 shows the axial distribution map of the liquid flow rates in the balance chamber at the positions of 0°, 90°, 180°, and 270° when the balance hole diameters are 0, 4, 6, 8, 10, and, 12 mm, respectively, under the designed working condition.

Table 2 shows the average values of the velocity in the balance chamber at the positions of 0°, 90°, 180°, and 270° when the balance hole diameters are 0, 4, 6, 8, 10, and, 12 mm. It could see the order of magnitude of this field.

As seen in Figure 6 and Table 2, the absolute velocity of the balance chamber liquid increases with radius at four angles (0°, 90°, 180°, and 270°) when there is no balance hole ($d = 0$ mm), which is due to the combined action of the impeller cover plate wall rotation and the hub rotation (as well as the obvious radial liquid velocity gradient). In addition, the closer to the sealing ring, the faster the velocity increases. The absolute axial velocity increases slightly near the impeller cover plate wall and involves a reduction area on the static pump cover plate wall. However, the velocity generally shows mild axial changes; specifically, there exists a core flow area with mild axial changes between the two boundary layers [16]. When the balance hole ($d > 0$ mm) exists, the distributions of absolute velocity are asymmetric at four angles (0°, 90°, 180°, and 270°) in the balance chamber, and the absolute velocity in the balance hole area is significantly higher. When the balance hole diameter increases from 4 mm to 12 mm, the absolute velocity decreases in the balance hole area but increases in the balance chamber,

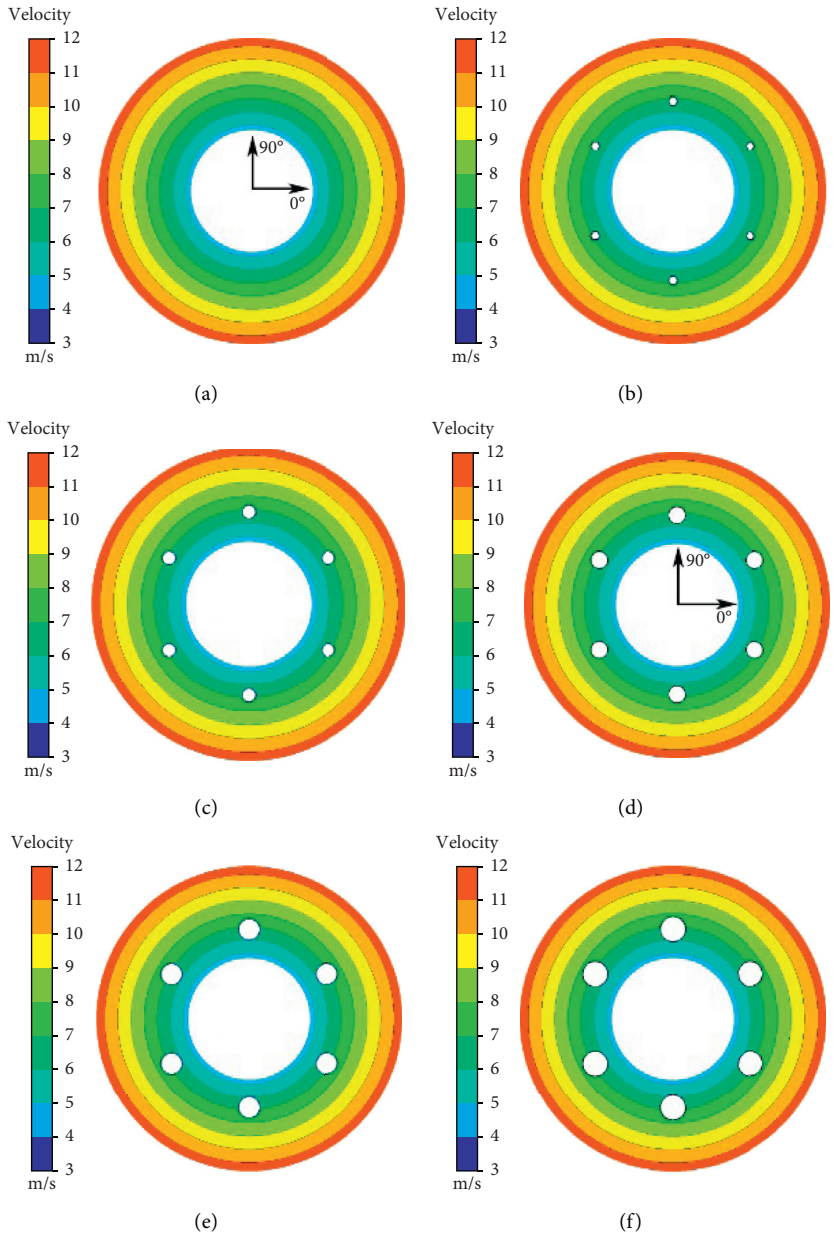

Figure 2: Velocity distribution of rotating wall in the balance chamber. (a) $d = 0$ mm; (b) $d = 4$ mm; (c) $d = 6$ mm; (d) $d = 8$ mm; (e) $d = 10$ mm; (f) $d = 12$ mm.

especially for the area of high velocity. When the balance hole diameter equals 8 mm, 10 mm, and 12 mm, the absolute liquid velocity in the balance hole area is almost equivalent to the value of the high velocity region in the balance chamber.

To study the ratio of balance chamber liquid velocity to impeller rotation velocity, the nondimensional tangential velocity $\overline{v}_u = (v_u/(\omega r))$, nondimensional radial velocity $\overline{v}_r = (v_r/(\omega r))$, and nondimensional radial length coefficient $\overline{r} = (r/(D/2))$ are introduced. Here, v_u represents the tangential velocity at the inner measuring point in the balance chamber, v_r is the radial velocity at the inner measuring point in the balance chamber, ω is the angular velocity of the impeller, and r is the radius at the measuring point. Figures 7 and 8 plotted the distribution of $\overline{v}_u$ and $\overline{r}$ at the axial center of the balance chamber in the designed working conditions when the balance hole diameters were 0, 4, 6, 8, 10, and 12 mm.

The increase of $\overline{v}_u$ within the two end-wall boundary regions was shown to be equivalent at each balance hole diameter. This is due to the rotation of the inner sealing ring wall and the hub, as well as the existence of a large positive (i.e., liquid flows from the hub toward the sealing ring) area of nondimensional radial velocity components $\overline{v}_r$ at a 90° direction near the hub area ($0 < \overline{r} < 0.2$). However, it is worth noting that a significant negative $\overline{v}_r$ region (the liquid flows from the sealing ring toward the hub) is found at a 270° direction in the $0.2 < \overline{r} < 0.6$ area; namely, the liquid flows

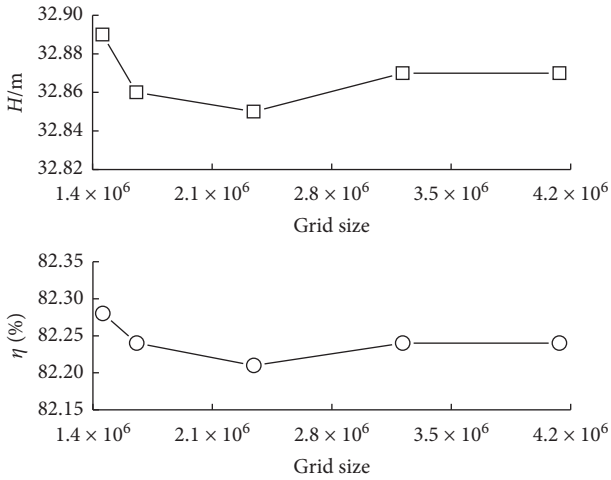

Figure 3: Grid independence verification.

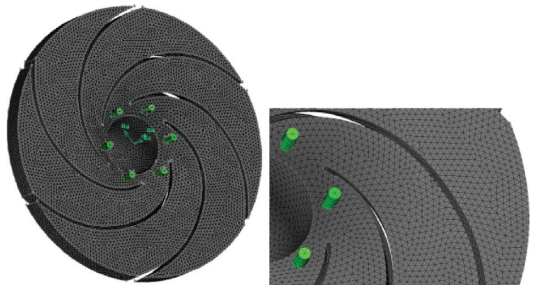

Figure 4: Grid of impeller model.

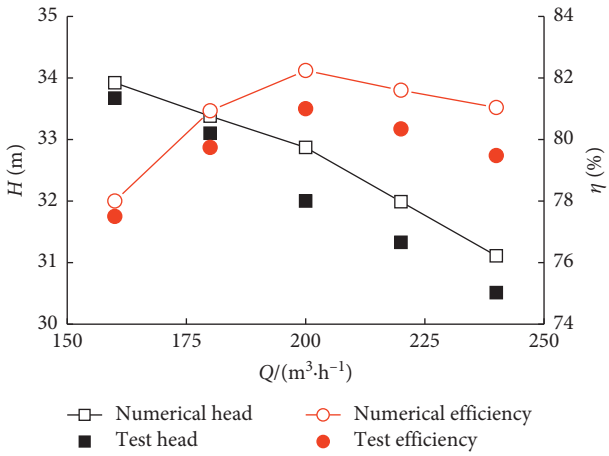

Figure 5: The performance curves of the centrifugal pump.

from the sealing ring toward the hub. When $\overline{r} > 0.6$, $\overline{v}_u$ or $\overline{v}_r$ values at four angles (0°, 90°, 180°, and 270°) are approximately equal. When $d = 0$ mm, the variation in trend of $\overline{v}_u$ and $\overline{v}_r$ at an equivalent radius at four angles (0°, 90°, 180°, and 270°) is generally consistent and axisymmetric, with a slight difference in distribution. When $d > 0$ mm, the radial distributions of $\overline{v}_u$ and $\overline{v}_r$ present significant differences at $\overline{r} < 0.6$ and at four different angles (0°, 90°, 180°, and 270°). The velocity shows the largest change at a 90° direction and the smallest change at a 0° direction; the maximum value is always at approximately $\overline{r} = 0.1$. Moreover, a larger balance hole diameter would lead to a higher value of $\overline{v}_u$ at the equivalent radius, and $\overline{v}_r$ will always approach zero. When the balance hole diameter increases from 1 mm to 12 mm, the difference in the overall distribution of $\overline{v}_u$ and $\overline{v}_r$ at an equivalent radius and four angles (0°, 90°, 180°, and 270°) increases first and then decreases later. The abovementioned phenomenon is due to the radial leakage flow of the balance hole ($0.17 < \overline{r} < 0.45$) area. The coeffect of the radial leakage flow from the seal clearance and impeller wall, the sealing ring inner wall, and hub rotation certainly influences the liquid flow rate in the balance chamber, leading to the significant difference in the distribution of $\overline{v}_u$ and $\overline{v}_r$ at four angles (0°, 90°, 180°, and 270°). This makes it difficult to achieve a consistent distribution.

Based on the above analysis, the significant changes in radial velocity distribution were at a 90° angle in the balance chamber. Figure 9 shows a liquid streamline track at a 90° angle in the balance chamber for further analysis.

From Figure 9, the liquid involves radial upward flow on the impeller wall and radial downward shear flow on the pump cover wall at an equivalent balance hole diameter due to the impeller rotation and static pump cover. In addition, several vortex areas are formed in the chamber, in which the vortex area at the seal clearance has a larger area. When $d = 0$ mm, the flow at the seal clearance is weaker than in other cases. When $d > 0$ mm, radial leakage flow from the balance chamber toward the impeller inlet occurs in the balance hole area, and obvious radial leakage can be observed from the seal clearance. When d increases from 0 mm to 8 mm, the center of vortex A first moves towards the lateral path of the sealing ring and then towards the side shaft of the impeller, thus generating vortex E below it. Vortex B gradually moves toward the pump cover below vortex A with an increase in the vortex intensity. Vortex C moves toward vortex D and combines with it, generating a new vortex F. Leakage vortex G at the seal clearance is gradually formed, and the vortex strength gradually increases. When d increases from 8 mm to 12 mm, the vortex structure and center position remain unchanged, and the strength of the interval leakage vortex G remains stable. The abovementioned strength of the seal clearance leakage vortex is consistent with the leakage amount variation rules shown in Figure 6. Vortex distribution rules in the balance chamber are consistent with the distribution rules in the high velocity area, as shown in Figures 6–8. The balance hole diameter $d = 8$ mm is a design value, where the above analysis proves the rationality of the design.

3.2. Validation of Leakage in the Balance Chamber. A study found that four pressure holes were made at radii of $r_1 = 62$ mm, $r_2 = 110$ mm, $r_3 = 130$ mm, and $r_4 = 155$ mm on the impeller back cover plate [18]. The rear chamber pressure and balance chamber pressure were measured with a YB-150 standard pressure gauge (0.5 grade precision). The air in the standard pressure gauge was

Table 1: The numerical results of performance parameters.

Balance hole diameter d (mm)	Flow Q (m^3/h)	Head H (m)	Efficiency η (%)
0	200	33.25	83.07
4	200	32.97	82.57
6	200	32.88	82.30
8	200	32.87	82.24
10	200	32.86	82.18
12	200	32.86	80.43

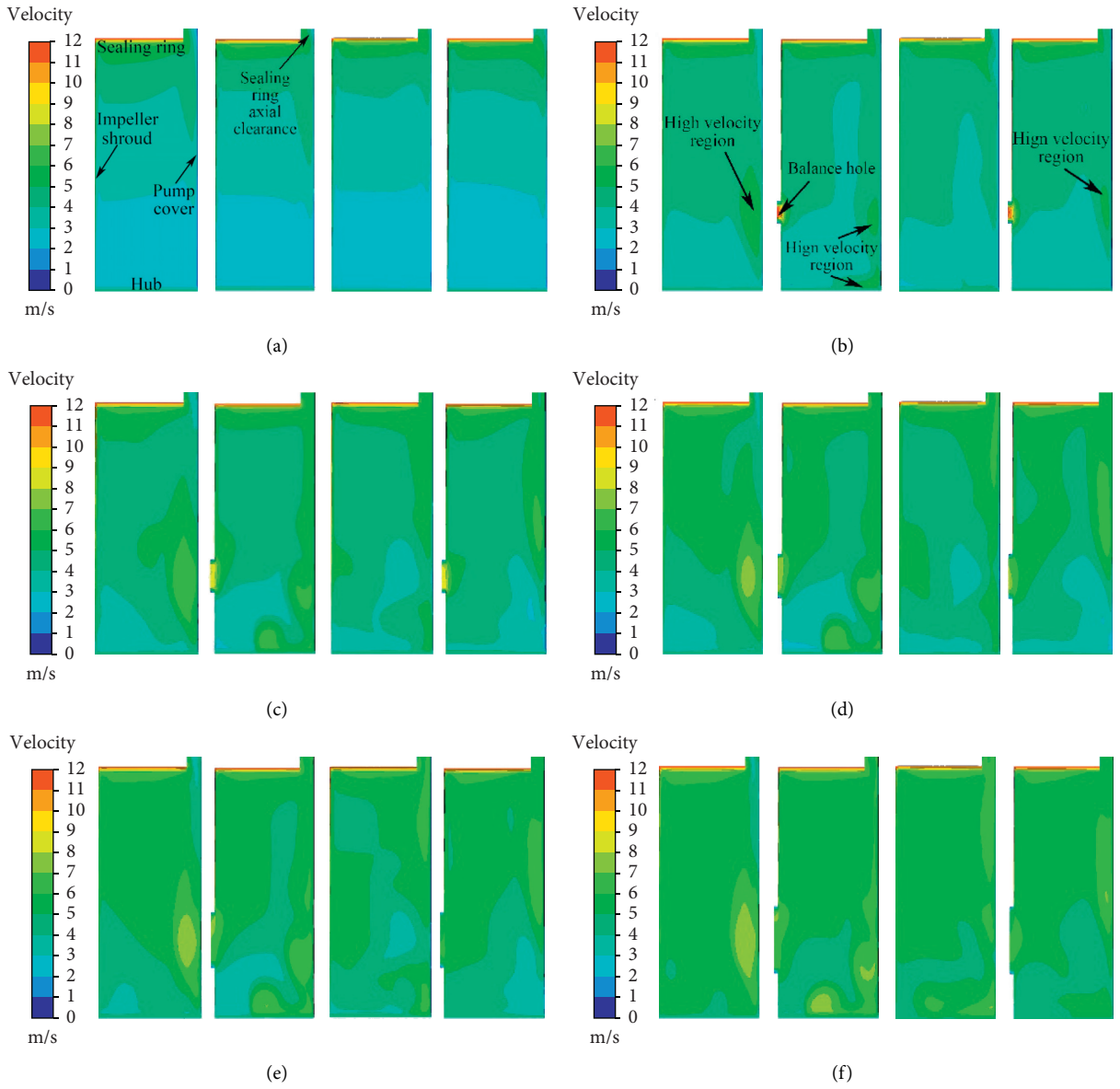

Figure 6: Axial distribution of absolute velocity in the balance chamber. (a) $\alpha = 0°$; (b) $\alpha = 90°$; (c) $\alpha = 180°$; (d) $\alpha = 270°$.

Table 2: The average values of absolute velocity.

Balance hole diameter d (mm)	0° (m/s)	90° (m/s)	180° (m/s)	270° (m/s)	Average values (m/s)
0	0.447	0.445	0.439	0.432	0.441
4	0.552	0.537	0.541	0.538	0.542
6	0.632	0.589	0.587	0.615	0.606
8	0.734	0.695	0.702	0.703	0.709
10	0.736	0.708	0.703	0.704	0.713
12	0.737	0.719	0.709	0.705	0.718

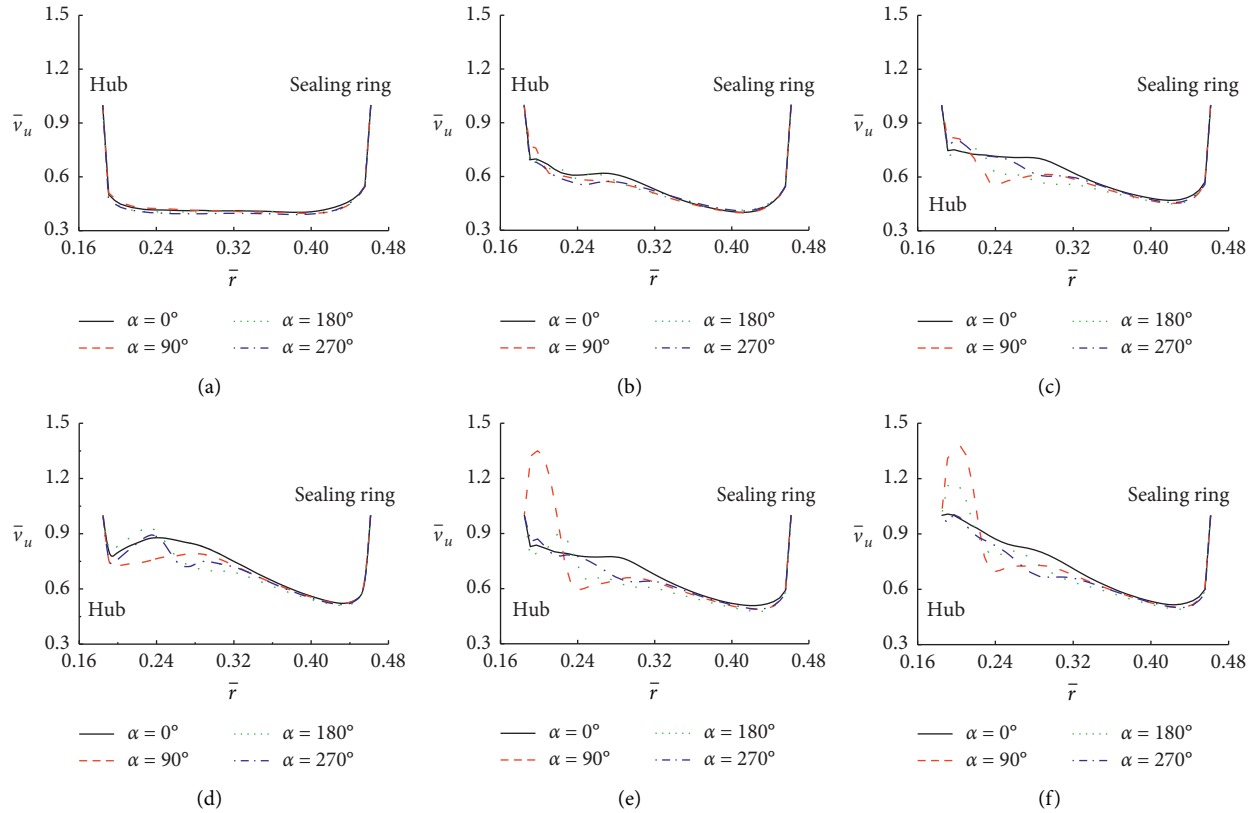

FIGURE 7: Radial distribution of dimensionless tangential velocity in the chamber. (a) $d = 0$ mm; (b) $d = 4$ mm; (c) $d = 6$ mm; (d) $d = 8$ mm; (e) $d = 10$ mm; (f) $d = 12$ mm.

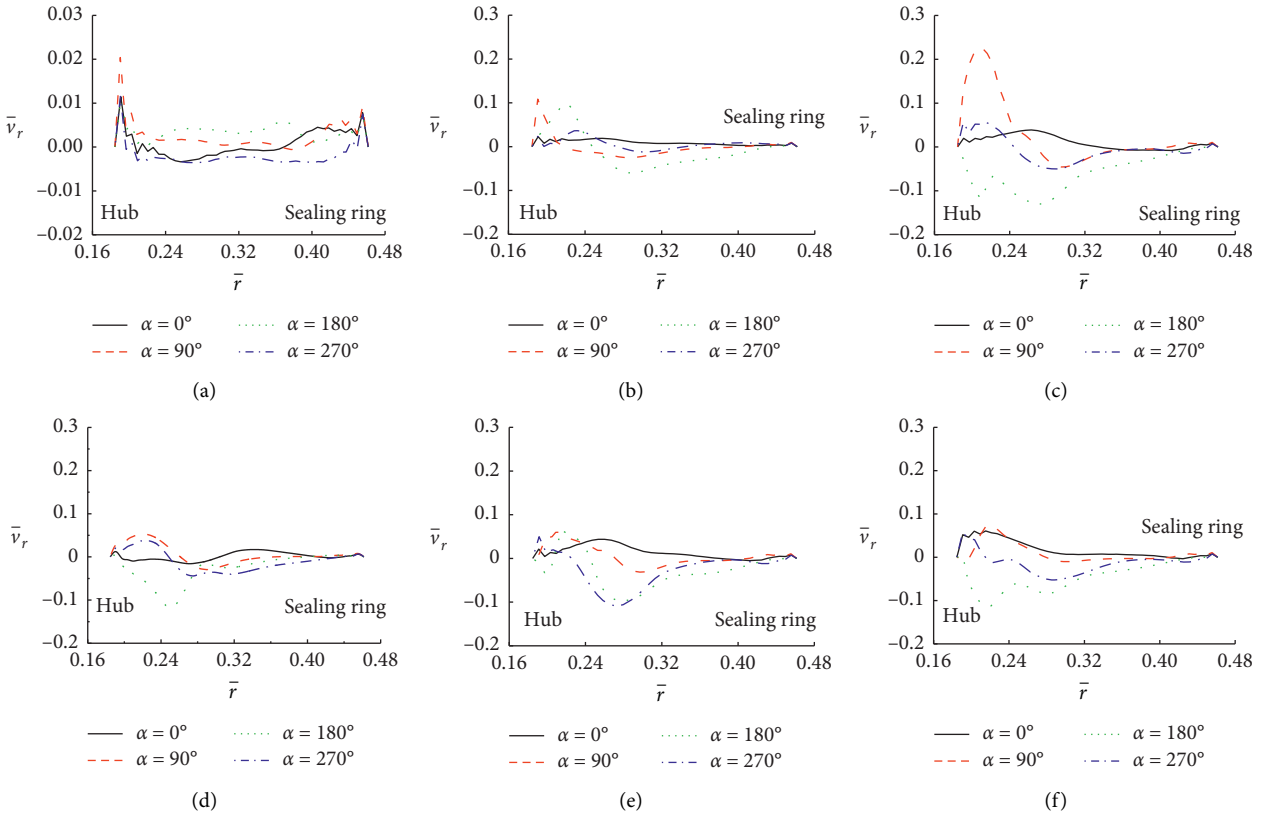

FIGURE 8: Radial distribution of dimensionless radial velocity in the chamber. (a) $d = 0$ mm; (b) $d = 4$ mm; (c) $d = 6$ mm; (d) $d = 8$ mm; (e) $d = 10$ mm; (f) $d = 12$ mm.

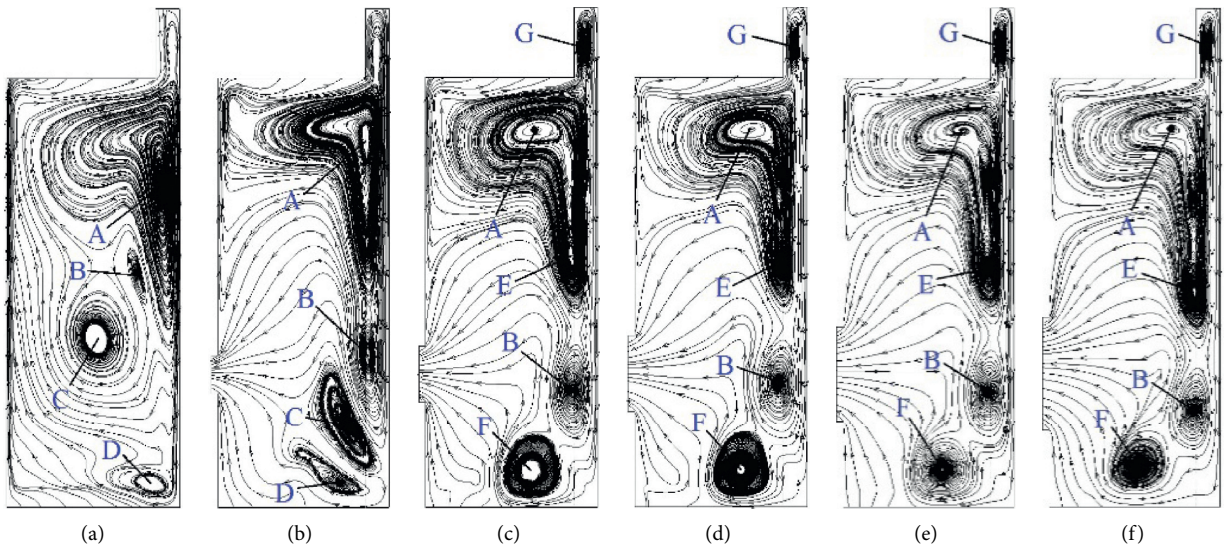

FIGURE 9: Streamline in the balance chamber at the 90°. (a) d = 0 mm; (b) d = 4 mm; (c) d = 6 mm; (d) d = 8 mm; (e) d = 10 mm; (f) d = 12 mm.

exhausted before the test to make the reading stable. The volume flow rate was measured with a LWGY-DN150 intelligent turbine flow meter. Real-time flow display was also provided. Figure 10 shows the measurement point on the rear chamber. The pressure value is the static pressure measured by the pressure gauge at standard atmospheric pressure.

In the pressure experiment, the size of the impeller radius was 162.5 mm and the hub radius was 30 mm; the experimental conditions were also taken into account. Therefore, the pressure values at the four radii were selected for measurement, which was sufficient to verify the accuracy of the numerical calculation results in this study. Figure 11 compares the computational and experimental values of pressure at the four radii. The computational value of pressure at each of the four radii is estimated by the average pressure at four angles, i.e., 0°, 90°, 180°, and 270°.

From Figure 11, the trend of numerical results is generally consistent with the test results. The relative error between the numerical result and the test result is 3.77% at r_4 = 155 mm. A certain pressure difference exists between the rear chamber and the balance chamber, with the former being higher than the latter. Therefore, driven by the pressure difference, the liquid in the rear chamber will enter the balance chamber through the back seal clearance, and the liquid in the balance chamber leaks into the impeller inlet through the balance hole. The volume flow rate of leakage in the back seal clearance and the balance hole gained after numerical calculation is shown in Table 3. The numerical result of the volume flow rate is usually given to three decimal places in the software FLUENT.

Table 3 indicates that the volume flow rate of the leakage flow from the balance hole q_{v1} is equal to that in the back seal clearance q_v at six balance hole diameters, which proves that the balance hole leakage flow changes the pressure difference between the balance and the rear chamber. This in turn leads to the production of back seal clearance leakage [8]. At the

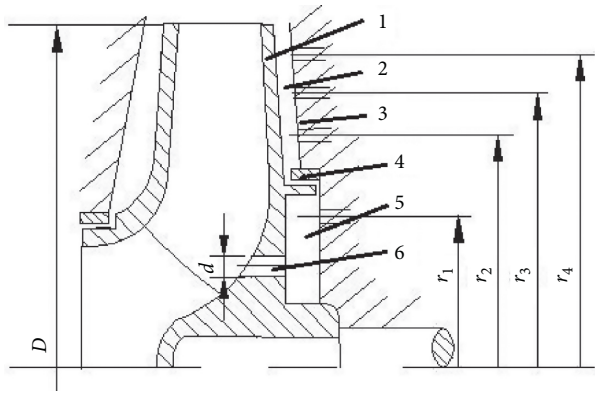

FIGURE 10: Positions of pressure measurements on the rear chamber. 1: impeller cover; 2: rear chamber; 3: pump cover; 4: impeller seal; 5: balance chamber; 6: balance hole.

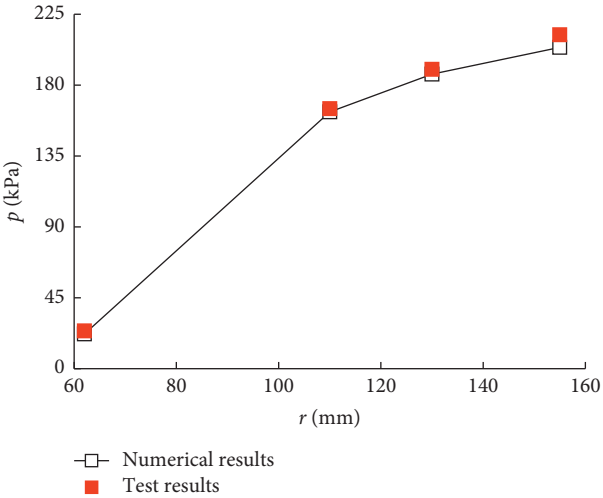

FIGURE 11: The comparison of predicted pressure and test results.

Table 3: Liquid leakage rate.

Balance hole diameter d (mm)	Back sealing ring q_v ($m^3 \cdot h^{-1}$)	Balance hole q_{v1} ($m^3 \cdot h^{-1}$)
0	0	0
4	2.093	2.093
6	3.388	3.388
8	3.746	3.746
10	3.855	3.855
12	3.864	3.864

same time, in the numerical simulation, the flow in the balance chamber is circumferential flow in the pump, which conforms to the law of mass conservation and the first law of thermodynamics. Under the designed working conditions, a larger balance hole diameter would increase the leakage flow from the back seal clearance. When $d < 8$ mm, the pressure difference between the balance chamber and the rear chamber increases with an increase in the balance hole diameter (the pressure in the latter is higher than that in the former), and the volume flow rate of leakage increases. When $d \geq 8$ mm, the radial pressure difference between the balance chamber and the rear chamber gradually becomes stable, with mild changes in the amount of leakage. In addition, $d = 8$ mm is the design value of the centrifugal pump balance hole diameter, indicating that the results of this paper are reliable.

A study conducted a characteristic test of the leakage volume flow rate in the balance chamber on a closed-type testing bed of the pump under two circumstances, i.e., the centrifugal pump with and without a balance hole ($d = 0$ mm and $d = 8$ mm) [18]. The volume flow rate of leakage in the centrifugal back seal clearance was calculated by combining the pressure values at the impeller back cover plate lateral chamber with radii of $r_1 = 62$ mm and $r_2 = 110$ mm, as measured in the test and the theoretical formula. This paper has adopted the geometrical characteristic parameter to reflect the balance hole diameter and number, back sealing ring diameter, and radial interval. We also adopted the percentage of the seal clearance leakage in the flow to analyze the relationship between the balance hole area and the leakage amount in the seal clearance in a similar pump [18].

The geometrical characteristic parameter $\overline{k}$ is

$$\overline{k} = \frac{d^2 z}{4 D_n b}, \tag{1}$$

and the percentage of seal clearance leakage in the flow $\overline{q}$ is

$$\overline{q} = \frac{q_v}{Q} \times 100\%. \tag{2}$$

Figure 12 indicates that the relative difference between the numerical results and the results derived from the experiment is 0.7% when no balance hole ($\overline{k} = 0$) exists. When a balance hole ($\overline{k} = 2.645$) exists, the relative difference is merely 0.12%. This can be explained by the fact that the axial force on the centrifugal pump impeller changes when no balance hole exists during the test. A slight axial movement and axial impeller-pump-cover interval value results in a certain leakage amount when no balance hole exists; however, the leakage amount is less than that recorded at $\overline{k} = 0.661$. In the simulation performed in this paper, when the centrifugal pump impeller is fixed at an axial position

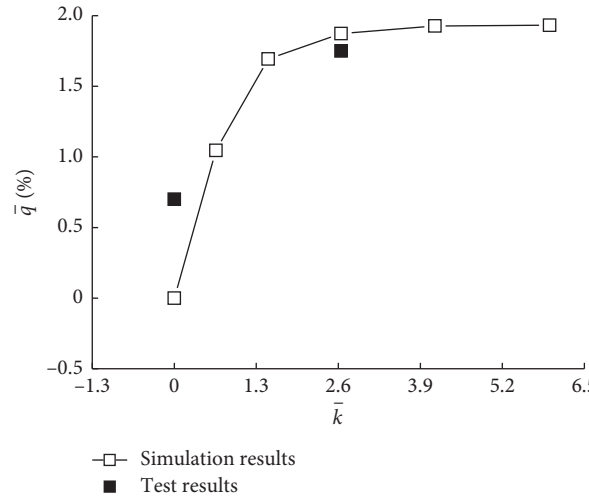

Figure 12: Dimensionless curve of leakage rate in the sealing ring.

and the axial interval value remains unchanged (with no balance hole involved $\overline{k} = 0$), the balance chamber is similar to a closed cylinder with its leakage amount approaching zero. As a result, the calculated volume flow rate of the balance chamber leakage flow is less than that obtained in the experimental results. Meanwhile, when $\overline{k}$ equals 2.645, the calculated result of the leakage amount in the balance chamber generally agrees with the test result, because the numerical results conform to the actual flow condition. In light of this, the simulation results of the leakage amount in the balance chamber are accurate and reliable, indicating that the calculation method adopted in this paper reflects the liquid flow characteristics in the balance chamber. Therefore, the CFD method is feasible.

The test data used to support the findings of this study are included within the paper.

4. Conclusions

The balancing holes in centrifugal pumps with seals mounted in both suction and discharge sides are one of the approaches used by pump manufacturers to reduce the axial thrust. The balance chamber has not been sufficiently studied due to the small axial radial dimensions and the complicated liquid flow in the cavity. However, the liquid flow characteristics in the equilibrium chamber are closely related to the diameter of the balance hole, which directly affects the axial force of the centrifugal pump. This paper focuses on the diameter of the balancing hole, and the results show that after the balance hole diameter increases to a certain value,

the balance hole leakage amount is about 2% of the flow rate and the axial force remains stable or substantially balanced. Studying the influence of the balance hole diameter on the liquid leakage, flow velocity, and vortex motion in the equilibrium cavity reveals the mechanism of the axial force and flow loss of the centrifugal pump. This is of great significance for accurately calculating and balancing the axial force.

When the balance hole area ratio $\overline{k} < 2.645$, the leakage amount ratio $\overline{q}$ is proportional to $\overline{k}$. When $\overline{k} \geq 2.645$, $\overline{q} \approx 2\%$, and the axial force remains stable (i.e., balanced).

Within the balance hole range of 0 mm to 12 mm, a larger balance hole diameter leads to a lower liquid flow rate in the balance hole but a higher liquid flow rate in the balance chamber.

The radial leakage flow of the back seal clearance and axial leakage flow of the balance hole result in changes in liquid flow rate, vortex center position, vortex structure, and vortex strength in the balance chamber. Therefore, these are the main factors influencing liquid flow rules in the balance chamber.

When $\overline{k} < 2.645$, a larger balance hole diameter would induce a stronger leakage from the seal clearance. When $\overline{k} \geq 2.645$, the vortex position, vortex structure, and vortex strength generally remain the same.

Data Availability

The data used to support the findings of this study are included within the article.

Conflicts of Interest

The authors declare no conflicts of interest.

Acknowledgments

This research was funded by the "National Natural Science Foundation of China, under No. 52009114," "Science and Technology Plan Project Funds for Shaanxi Provincial Department of Water Resources, under No. 2019slkj-15," "Basic Natural Science Research Program of Shaanxi Province, under No. 2019JLM-58," and "Fundamental Research Funds for the Central Universities, under No. Z1090219041."

References

[1] W. Li, "Model of flow in the side chambers of an industrial centrifugal pump for delivering viscous oil," *Journal of Fluids Engineering-Transactions of the ASME*, vol. 135, no. 5, Article ID 051201, 2013.

[2] B. Shi and J. Wei, "Numerical simulation of 3D solid-liquid turbulent flow in a low specific speed centrifugal pump: performance comparison of four geometric models," *Advances in Mechanical Engineering*, vol. 6, Article ID 678271, 2014.

[3] H. M. Badr and W. H. Ahmed, "Axial and radial thrusts in centrifugal pumps," *Pumping Machinery Theory and Practice*, pp. 133–158, Wiley, Hoboken, NJ, USA, 2014.

[4] M. Gao, P. Dong, S. Lei, and A. Turan, "Computational study of the noise radiation in a centrifugal pump when flow rate changes," *Energies*, vol. 10, no. 2, p. 221, 2017.

[5] X. Han, Y. Kang, D. Li, and W. Zhao, "Impeller optimized design of the centrifugal pump: a numerical and experimental investigation," *Energies*, vol. 11, no. 6, p. 1444, 2018.

[6] Y.-D. Choi, J. Kurokawa, and J. Matsui, "Performance and internal flow characteristics of a very low specific speed centrifugal pump," *Journal of Fluids Engineering*, vol. 128, no. 2, pp. 341–349, 2006.

[7] A. F. Ayad, H. M. Abdalla, and A. A. El-Azm Aly, "Effect of semi-open impeller side clearance on the centrifugal pump performance using CFD," *Aerospace Science and Technology*, vol. 47, pp. 247–255, 2015.

[8] B.-C. Will, F.-K. Benra, and H.-J. Dohmen, "Investigation of the flow in the impeller side clearances of a centrifugal pump with volute casing," *Journal of Thermal Science*, vol. 21, no. 3, pp. 197–208, 2012.

[9] W.-D. Cao, X. Dai, and Q.-X. Hu, "Effect of impeller reflux balance holes on pressure and axial force of centrifugal pump," *Journal of Central South University*, vol. 22, no. 5, pp. 1695–1706, 2015.

[10] T. Shimura, S. Kawasaki, M. Uchiumi, T. Kimura, and J. Matsui, "Internal flow and axial thrust balancing of a rocket pump," *Journal of Fluids Engineering-Transactions of the ASME*, vol. 134, no. 4, Article ID 041103, 2012.

[11] X.-Y. Ji, X.-B. Li, W.-T. Su, X. Lai, and T.-X. Zhao, "On the hydraulic axial thrust of francis hydro-turbine," *Journal of Mechanical Science and Technology*, vol. 30, no. 5, pp. 2029–2035, 2016.

[12] J. Park, Y. Shin, and J. Chung, "Performance prediction of centrifugal compressor for drop-in testing using low global warming potential alternative refrigerants and performance test codes," *Energies*, vol. 10, no. 12, p. 2043, 2017.

[13] H. Zhang, S. Deng, and Y. Qu, "Numerical investigation of periodic fluctuations in energy efficiency in centrifugal pumps at different working points," *Energies*, vol. 10, no. 3, p. 342, 2017.

[14] S. Tang, S. Yuan, and Y. Zhu, "Deep learning-based intelligent fault diagnosis methods toward rotating machinery," *IEEE Access*, vol. 8, no. 1, pp. 9335–9346, 2020.

[15] H. Liu, K. Wang, S. Yuan, M. Tan, Y. Wang, and L. Dong, "Multicondition optimization and experimental measurements of a double-blade centrifugal pump impeller," *Journal of Fluids Engineering-Transactions of the ASME*, vol. 135, no. 1, Article ID 011103, 2012.

[16] D. Bonaiuti, M. Zangeneh, R. Aartojarvi, and J. Eriksson, "Parametric design of a waterjet pump by means of inverse design, CFD calculations and experimental analyses," *Journal of Fluids Engineering-Transactions of the ASME*, vol. 132, no. 3, Article ID 031104, 2010.

[17] R. Debuchy, F. A. Nour, and G. Bois, "An analytical modeling of the central core flow in a rotor-stator system with several preswirl conditions," *Journal of Fluids Engineering-Transactions of the ASME*, vol. 132, no. 6, Article ID 061102, 2010.

[18] W. Jörn, B. Friedrich, and D. Hans, "Investigation of the flow in the impeller side clearances of a centrifugal pump with volute casing," *Journal of Thermal Science*, vol. 21, no. 3, pp. 197–208, 2012.

[19] W. Dong and W. Chu, "Numerical investigation of the fluid flow characteristics in the hub plate crown of a centrifugal pump," *Chinese Journal of Mechanical Engineering*, vol. 31, no. 1, p. 64, 2018.

[20] T. Capurso, L. Bergamini, and M. Torresi, "Design and CFD performance analysis of a novel impeller for double suction centrifugal pumps," *Nuclear Engineering and Design*, vol. 341, pp. 155–166, 2019.

[21] M. F. Khalil, S. Z. Kassab, A. A. A. Naby, and A. Azouz, "Performance characteristics of centrifugal pump conveying soft slurry," *American Journal of Mechanical Engineering*, vol. 1, no. 5, pp. 103–112, 2013.

[22] W. Li, "Effects of flow rate and viscosity on slip factor of centrifugal pump handling viscous oils," *International Journal of Rotating Machinery*, vol. 2013, Article ID 317473, 12 pages, 2013.

[23] S. Tang, S. Yuan, and Y. Zhu, "Convolutional neural network in intelligent fault diagnosis toward rotatory machinery," *IEEE Access*, vol. 8, no. 1, pp. 86510–86519, 2020.

[24] T. Mihalic, Z. Guzovic, and A. Predin, "Performances and flow analysis in the centrifugal vortex pump," *Journal of Fluids Engineering-Transactions of The ASME*, vol. 135, no. 1, Article ID 011107, 2013.

[25] N. Zhang, M. Yang, B. Gao, and Z. Li, "Vibration characteristics induced by cavitation in a centrifugal pump with slope volute," *Shock and Vibration*, vol. 2015, Article ID 294980, 10 pages, 2015.

[26] Q. Si, G. Bois, Q. Jiang, W. He, A. Ali, and S. Yuan, "Investigation on the handling ability of centrifugal pumps under air-water two-phase inflow: model and experimental validation," *Energies*, vol. 11, no. 11, p. 3048, 2018.

[27] Y. Yang, L. Zhou, W. Shi, Z. He, Y. Han, and Y. Xiao, "Interstage difference of pressure pulsation in a three-stage electrical submersible pump," *Journal of Petroleum Science and Engineering*, vol. 196, Article ID 107653, 2020.

[28] B. Xia, F. Y. Kong, H. Zhang, L. Yang, and W. H. Qian, "Investigation of axial thrust deviation between the theory and experiment for high-speed mine submersible pump," *Advances in Mechanical Engineering*, vol. 10, no. 8, pp. 1–13, 2018.

[29] L. Zhou, C. Han, L. Bai, W. Li, M. El-Emam, and W. Shi, "CFD-DEM bidirectional coupling simulation and experimental investigation of particle ejections and energy conversion in a spouted bed," *Energy*, vol. 211, Article ID 118672, 2020.

[30] X. Jia, B. Cui, Z. Zhu, and X. Yu, "Numerical investigation of pressure distribution in a low specific speed centrifugal pump," *Journal of Thermal Science*, vol. 27, no. 1, pp. 25–33, 2018.